BNL-NUREG-29510
CONF-810804--7

A NONEQUILIBRIUM VAPOR-GENERATION MODEL FOR FLASHING FLOWS*

P. Saha, N. Abuaf† and B. J. C. Wu††
Department of Nuclear Energy
Brookhaven National Laboratory
Upton, New York

BNL-NUREG--29510

TI85 018228

ABSTRACT

A nonequilibrium vapor generation model for flashing flows is presented. The model consists of a flashing inception point, a bubbly flow regime followed by a bubbly-slug regime, an annular or annular-mist regime, and finally a dispersed-droplet regime. Existence of superheated liquid at the inception point and beyond is recognized. The vapor generation rate in each flow regime is calculated from the estimates for interfacial area density and net interfacial heat flux. However, the bubble number density at the flashing inception point was varied to obtain optimum fits with the void fraction data taken in a vertical converging-diverging nozzle. The interfacial area density at the inception point, thus determined, showed a rapid increase with the decrease in the liquid superheat at that point. This trend is correct since in the limit of thermal equilibrium flow where the liquid superheat approaches zero, the interfacial area for heat and mass transfer should approach infinity.

† Present Address: General Electric Co., Schenectady, New York
†† Present Address: Lawrence Livermore National Laboratory, Livermore, Calif.
* Work performed under the auspices of the U. S. Nuclear Regulatory Commission

MGW/JSW

DISCLAIMER

NOMENCLATURE

A	cross sectional area, m^2
a	thermal diffusivity, m^2/s
a_i	interfacial area density, m^2/m^3
C_1	constant used in Equation (11)
C_3	constant used in Equation (42)
c_p	specific heat at constant pressure, J/kg K
D	pipe or channel diameter, m
d	droplet diameter, m
f	parameter used in Equation (26)
G	mass flux, kg/m^2s
G_g	vapor mass flux, kg/m^2s
g	acceleration due to gravity, m/s^2
h	specific enthalpy, J/kg
	heat transfer coefficient, W/m^2K
J	nucleation rate, $1/m^2s$
k	thermal conductivity, W/mK
L	latent heat of vaporization, J/kg
	length, m
N_b	bubble number density, $1/m^3$
Nu	Nusselt number
Pe	Peclet number
Pr	Prandtl number
p	pressure, N/m^2
q''_i	interfacial heat flux, W/m^2
R_{cr}	critical bubble radius, m
R_T	radius of Taylor bubble, m
St	Stanton number
T	temperature, K
t	time, s
V	volume, m^3
v	velocity, m/s
$v_{g\ell}$	relative velocity between vapor and liquid, m/s
v_{gj}	vapor drift velocity, m/s
We	Weber number
X	flow quality
Z	axial coordinate, m
α	void fraction

Γ_v volumetric rate of vapor mass generation, kg/m^3s

ξ_h perimeter, m

λ_T length-to-diameter ratio of Taylor bubble

ρ density, kg/m^3

μ viscosity, kg/ms

σ surface tension, N/m

ω equivalent sphere radius, m

SUBSCRIPTS

b bubble or bubbly flow regime

c unit cell

d droplet

g saturated vapor

i vapor-liquid interface

ℓ liquid

m mixture

o flashing inception point

s bubbly-slug flow regime

sat saturation

ss steady state

T throat, Taylor bubble

v vapor

INTRODUCTION

Flashing of liquid to a two-phase mixture through pipes and nozzles is an important phenomenon in the area of nuclear reactor safety, energy conversion and space propulsion, among others. The analysis of such flows becomes difficult, particularly for short pipes and nozzles, because of the nonequilibrium aspect of phase change (1). The transition from liquid to vapor-liquid two-phase flow by flashing usually takes place in several stages. First, the pressure drop experienced by the initially subcooled flowing liquid must be sufficient to bring the liquid to a saturated state. However, vaporization does not occur upon reaching the saturation state, because a finite liquid-to-vapor temperature difference is required for phase change. Therefore, the liquid becomes superheated as the pressure decreases further and falls below the saturation value.

Second, bubble nucleation, either homogeneously or heterogeneously, begins after an "induction" period when a certain liquid superheat has been attained. The degree of superheat required for nucleation may depend on the flow conditions and the time rate of depressurization. Because of the strong dependence of nucleation rate on the thermodynamic state of the parent phase, small changes in the liquid superheat may drastically affect the bubble nucleation rates. Therefore, bubble nucleation rates will rise quickly to a peak value after the liquid superheat increases above a "threshold" value. However, the formation of these thermodynamically stable vapor nuclei and the accompanying loss of latent heat by the liquid to the vapor is expected to decrease the liquid superheat slightly so as to cause the nucleation rate to decline to a much lower value. The width of the nucleation zone is a function of the physical properties of the liquid and vapor, the flow velocity, the depressurization rate, and other flow variables. In the case of condensation in supersonic flows, it has been found by Wegener and Wu (2) , that the nucleation zone is only a few millimeters wide, and the transport time across this zone is of the order of 10 us. However, it is not clear how wide the bubble nucleation zone is in flashing flows.

Third, vaporization of the liquid, which is still superheated at the surface of these dispersed bubbles, dominates the phase transition. This is the region of simple bubble growth. Finally, at a void fraction of about 30% the bubble coagulation becomes effective in substantially altering the bubble population and size distribution, leading eventually to bubbly-slug and annular-mist flow regimes.

Flashing in commercial pipes is most likely initiated by heterogeneous nucleation of vapor bubbles in the bulk liquid and/or at crevices or microcavities along the wall with pre-existing gas phase. Following Oswatitsch's treatment of condensation in supersonic nozzles (3), Zuber et al. (4) proposed a model which led to an expression for the calculation of the mass flow rate of vapor, G_g, over a cross section located at a point Z along a duct of constant cross section A:

$$G_g(Z) = \frac{1}{A} \int_{Z_o}^{Z} \xi_h m(Z,\zeta) J(\zeta) d\zeta \ , \qquad (1)$$

where ξ_h is the perimeter of the duct, $J(\zeta)$ is the nucleation rate per unit wall area at point ζ along the pipe, $m(Z,\zeta)$ is the mass at Z of a vapor bubble nucleated at ζ, and Z_o is a point upstream from the nucleation zone. The integration effectively sums the vapor mass of all the bubbles nucleated before point Z. Although Oswatitsch's model has been applied to the study of condensation in high speed flows with remarkable success (2), its extension to flashing flow has been difficult, mainly because of the lack of understanding of the heterogeneous nucleation process, and of the nucleation rates (J) for flashing flows.

Rohatgi and Reshotko (5) carried out such a calculation for flashing flow of liquid nitrogen and compared their results with the experimental results of Simoneau (6). There were two unknown parameters in their heterogeneous nucleation equations, one being the number of effective nucleation sites per unit area, and the other being the contact angle between liquid nitrogen and the surface of the heterogeneity. They determined these unknown parameters by "best-fits" to the experimental data, but they did not apply the analysis to any steam-water data.

To circumvent the above difficulty, Wu et al (7) treated the nucleation and bubble growth separately and proposed a conduction controlled vapor generation model which was first applied to the experimental data

of Reocreux (8). The local vapor generation rate depends primarily on three quantities which are unknown a priori:

a. the onset of flashing or inception point, z_{NVG},

b. the initial void fraction, α_o, at the point of inception; and

c. a quantity, C_r, which is related to the number of bubbles generated at the inception point.

The values of these three parameters were determined independently by the "best-fit" to the void fraction data (7). In reality they are all related to one another. For example, if the liquid superheat at the inception point is specified, both the flashing onset location, z_{NVG} and the critical bubble radius at the onset location can be determined. The value of the initial void fraction, α_o, is then uniquely related to the bubble number density at the inception point.

Semi-empirical correlations (9 and 10) are now available for determining the liquid superheat at the flashing inception point. This paper will, therefore, concentrate on discussing a mechanistic nonequilibrium vapor generation model applicable for the flashing two-phase flows. The model requires a priori knowledge of the liquid superheat at the flashing inception point and uses the bubble number density at the inception point as a "free" parameter. This parameter is then evaluated from the flashing experiment conducted in a vertical converging-diverging nozzle (11).

PRESENT MODEL

The heat transfer dominated vapor generation rate per unit volume following flashing inception can be given by:

$$\Gamma_v = a_i \dot{q}_i'' / L \qquad (2)$$

where a_i is the total liquid-vapor interfacial area per unit volume of the mixture, $\dot{q}_i''$ is the net heat flux to the interface, and L is the latent heat of vaporization. Both a_i and $\dot{q}_i''$ are flow regime dependent, and are functions of the thermodynamic state and flow variables. Therefore, to calculate a_i and $\dot{q}_i''$ it is necessary to know, a priori, in which flow regime the system is expected to be. In this model, a simple flow regime map for vertical flows is assumed where the flow regime is a function of the local void fraction only[1]. Thus, a bubbly flow, a bubbly-slug, an annular and/or annular-mist regime, and finally a dispersed droplet flow are assumed to occur at successively higher void fraction ranges, as shown in Figure 1. The void fractions at the transition points are assumed to be

$$\alpha_{b\ max} = 0.3, \quad \alpha_{s\ max} = 0.8, \quad \alpha_d = 0.95 .$$

[1] A more elaborate flow regime map may be used in the future if deemed necessary.

The interfacial area densities and the heat transfer coefficients applicable to interfacial heat transfer for each flow regime shown in Figure 1 are discussed below.

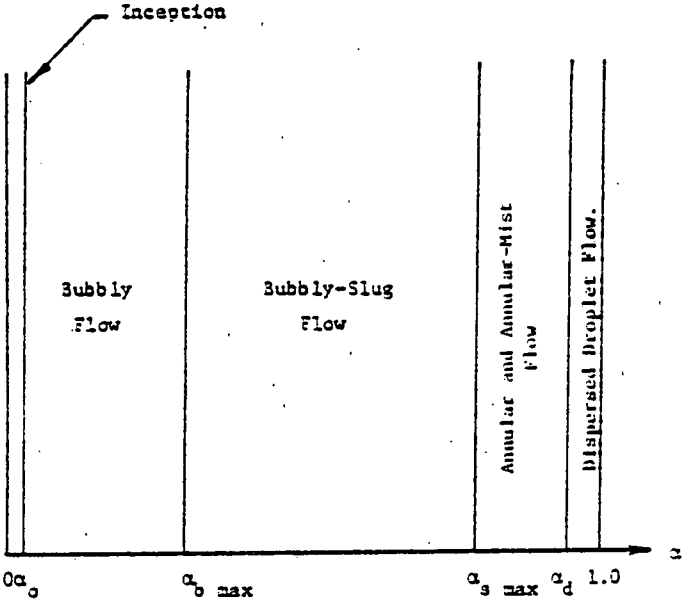

Figure 1. The Flow Regimes Map

Bubble Nucleation Zone, $0 < \alpha < \alpha_o$

The bubble nucleation zone is the point of flashing inception, and it serves as the starting point of the vapor generation calculation. It is assumed that a certain number of bubbles are nucleated in this "narrow" zone and the net vapor generation at a location downstream will be dominated by the bubbles nucleated in this zone. This assumption is supported by the work of Jones and Zuber (12) who found that the rate of bubble volume growth is a strong function of growth time. Therefore, the contributions of the bubbles nucleated downstream of the bubble nucleation zone or the flashing inception point is neglected in this study. This is similar to the assumption used by many of the earlier researchers (e.g., Edwards (13)).

The location of flashing inception may be determined either from the flashing inception correlations (9 and 10) or from experimental observation. At the inception point, the vapor is assumed to be in the form of critical sized bubbles, with radius R_{cr}:

$$R_{cr} = 2\sigma/(p_{sat}(T_\ell) - p) \qquad (3)$$

The critical radius is of the order of a few microns for typical liquid superheat (or pressure undershoot) values found experimentally at flashing inception. At these sizes the bubbles can certainly be considered to be spherical and to move with the liquid without slip. Thus the following expressions can be written to start the calculation for vapor generation:

$$\alpha_o = \frac{4\pi}{3} R_{cr}^3 N_{b,o} , \qquad (4)$$

$$a_{i,b} = 3\,\alpha_o/R_{cr} \quad (5)$$

$$X_o \simeq \alpha_o\,\rho_g/\rho_\ell \quad (6)$$

where X_o is the initial quality and $N_{b,o}$ is the number of bubbles per unit mixture volume at the inception point which may be related to the packing density (9) through the flow geometry.

Bubbly Flow

For $\alpha_o < \alpha < \alpha_{b,max}$, the flow is assumed to be in the bubbly regime. The vapor exists in the form of bubbles of uniform size, although not necessarily spherical. However, an equivalent sphere radius, ω, can be defined such that the bubble volume is written as

$$V = 4\pi\,\omega^3/3. \quad (7)$$

In general, the bubbles will move faster than the surrounding liquid. Because of the complexity of implementing a general form of the bubble rise velocity as prescribed by Wallis (14), a simplified form of the vapor drift velocity is adopted here:

$$v_{gj} = 1.41\left[\frac{g\sigma(\rho_\ell-\rho_g)}{\rho_\ell^2}\right]^{1/4} \quad (8)$$

if $\alpha > 0.3\sqrt{\sigma/(\rho_\ell g)}$. For $\alpha < 0.3\sqrt{\sigma/(\rho_\ell g)}$, a linear interpolation between zero and the above value is used. The relative velocity between the bubbles and the surrounding liquid is then calculated from

$$v_{g\ell} = v_{gj}/(1-\alpha) \quad (9)$$

For the interfacial heat transfer coefficient, it has been found (15) that even for bubble growth during a variable liquid superheat condition, the Plesset-Zwick (16) or Forster-Zuber (17) type of heat transfer coefficient may be used for short time. However, for a bubbly flow with relative velocity, these expressions should be modified in such a way that the convective heat transfer due to the relative velocity is also accounted for. The general expression should satisfy the limiting behavior of the heat transfer process at both $t \to 0$ and $t \to \infty$, where t is the time from bubble nucleation. At the inception point, the transient conduction dominates the heat transfer process so that the general expression should approach the Plesset-Zwick or Forster-Zuber expression at $t \to 0$. However, as the bubbles "age", the convective heat transfer due to the relative velocity between the bubbles and liquid starts to dominate, as shown by Wolfert (18). Therefore, at $t \to \infty$, the general expression should yield the steady-state convective heat transfer coefficient to the bubbles.

The steady state heat transfer rate to a spherical bubble moving at constant speed in an infinite liquid is given by the Boussinesque solution (19) which may be expressed as

$$Nu_{\ell,ss} = h_{ss}\cdot 2\,\omega/k_\ell = 2\sqrt{Pe_\ell/\pi} \quad (10)$$

where the subscript ss stands for steady-state bubble motion, and the bubble Peclet number is defined as $2v_{g\ell}\omega/a_\ell$. For a spherical cap, the heat transfer rate based on the surface area of the equivalent sphere is estimated to be about 20% higher than that for the sphere (20). This estimate agrees with the Calderbank and Lochiel's model (21) and it is in fair agreement with their experiments. Thus, in terms of the heat transfer coefficient based on the equivalent sphere,

$$h_{ss} = k_\ell\sqrt{\frac{C_1}{\pi}}\cdot\sqrt{\frac{v_{g\ell}}{\omega a_\ell}} \quad (11)$$

where $C_1 = 2.0$ for spheres

$= 2.38$ for spherical caps.

Two simple expressions are found in the literature which provide a smooth transition from the Plesset-Zwick expression at $t \to 0$ to the steady-state heat transfer coefficient at $t \to \infty$. These are:

$$h_\ell = \frac{\sqrt{3}\,k_\ell}{\sqrt{\pi a_\ell t}}\left[1 + \frac{C_1}{3}\,\frac{v_{g\ell}\,t}{\omega}\right]^{1/2} \quad (12)$$

and

$$h_\ell = \frac{\sqrt{3}\,k_\ell}{\sqrt{\pi a_\ell t}}\left[1 + \sqrt{\frac{C_1}{3}\,\frac{v_{g\ell}\,t}{\omega}}\right] \quad (13)$$

The first is due to Aleksandrov et al. (22) as modified by Saha (15) and the second to Wolfert (18). Since both of these expressions were based on intuitive physical arguments, it is not clear which is more realistic. Note, however, that Wolfert's expression always yields a greater value for h_ℓ. For the present calculations, the modified Aleksandrov expression (Equation 12) with $C_1 = 2.0$ is used.

The interfacial area density is calculated from the following expression:

$$a_{i,b} = 3\,\alpha/\omega \quad (14)$$

regardless of whether the bubbles are spheres or not. However, a method of calculating the variation of equivalent bubble radius, ω, and the void fraction, α, is required.

In the bubbly flow regime, it is assumed that no bubble coalescence or disintegration takes place. Thus, the bubble radius changes only as a result of vaporization or condensation at the interface,

$$\frac{d\omega}{dt} = \frac{q_i''}{L\rho_g} = \frac{h_\ell\,(T_\ell' - T_{sat})}{L\rho_g} \quad (15)$$

This equation is equivalent to Equation (2) written on the basis of unit interfacial area rather than unit volume. Also, the vapor phase is assumed to be at saturation.

To calculate the void fraction α, an equation for the conservation of bubble number for the bubbly flow regime was utilized. For steady-state, this equation results in the following simple expression:

$$N_b v_g A = \text{constant} = (N_b v_g A)_o \qquad (16)$$

The bubble density, N_b, can now be calculated at any cross section, and the void fraction can then be calculated from:

$$\alpha = \frac{4}{3} \pi \omega^3 N_b \ . \qquad (17)$$

The liquid superheat is calculated from the mixture energy equation by assuming the vapor phase to be at saturation, and the flow to be adiabatic,

$$h_m + \frac{1}{2} \left(\frac{G}{\rho_m} \right)^2 = \text{constant} \ . \qquad (18)$$

Bubbly-Slug Flow

As the void fraction increases, bubble coalescence becomes significant. Following Dukler and Taitel (23), it is assumed here that when $\alpha = \alpha_{b\ max} = 0.3$ some of the bubbles begin to coagulate to form larger bubbles, while the others continue to grow by vaporization according to the rate and mechanism discussed above. Thus, two classes of bubbles coexist in this flow regime; the larger bubbles formed by coagulation and the smaller original bubbles. As a result of vaporization at the interface, both classes of bubbles grow, although at different rates. As the coagulation increases, the number of the smaller bubbles decreases. The larger bubbles resulting from coagulation are probably not spherical. They may either approach the spherical cap shape, or, if ω is comparable to or greater than the pipe radius, they may acquire an elongated cylindrical shape with a rounded head. These latter bullet-shaped bubbles are called the Taylor bubbles, and they are usually separated by liquid (or bubbly-liquid) regions.

Since the vapor generation takes place on the surface of the Taylor bubbles as well as on the small bubbles, the vapor generation rate or the total heat transfer rate is the sum of the two components:

$$h\, a_i = h_T\, a_{i,T} + h_b\, a_{i,b} \ , \qquad (19)$$

where the subscripts T and b designate quantities pertaining to the Taylor bubbles and the small bubbles.

Figure 2, which illustrates the nomenclature for the bubbly-slug flow regime in a circular pipe, shows the Taylor bubbles, the unit cell in which one Taylor bubble may be found on the average, and the small bubbles in the bubbly-liquid zone between two consecutive Taylor bubbles. The Taylor bubbles are assumed to be cylinders of length $2\lambda_T R_T$ and radius R_T.

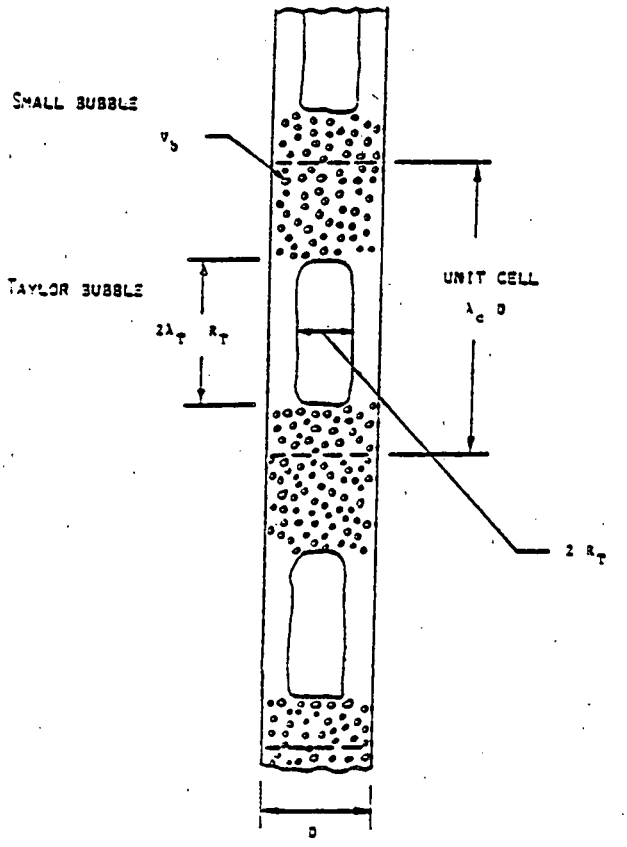

Figure 2. Nomenclature for Bubbly-Slug Flow.

It is also assumed that as the void fraction increases, the Taylor bubbles absorb (or suck in) the neighboring smaller bubbles and eventually merge with one another to form a continuous vapor core. This represents the end of the bubbly-slug regime and the beginning of the annular flow regime which has been assumed to occur at $\alpha = \alpha_{s\ max}$. Therefore, at $\alpha = \alpha_{s\ max}$,

$$\frac{2 R_T}{D} = \sqrt{\alpha_{s\ max}} \qquad \text{and} \qquad L_T = L_c \ . \qquad (20)$$

Assuming that the length-to-diameter ratio of the Taylor bubbles, λ_T, remains the same for the entire bubbly-slug region, the following expression can be derived for the length of the unit cell:

$$L_c = \lambda_T D \sqrt{\alpha_{s\ max}} \ . \qquad (21)$$

Therefore, the void fraction due to the Taylor bubbles alone is given by

$$\alpha_T = \frac{V_T}{V_c} = \frac{8 R_T^3}{\sqrt{\alpha_{s\ max}}\, D^3} \qquad (22)$$

and the interfacial area density due to the Taylor bubbles can be given by

$$a_{i,T} = 4\left(1 + \frac{1}{2\lambda_T}\right)\frac{\alpha_T^{2/3}}{\alpha_{s\,max}^{1/6} D} \quad . \tag{23}$$

Note that if the length-to-diameter ratio of the Taylor bubble is 5, the surface area of the two ends of the cylinder is only 10% of the total surface area. Moreover, the heat transfer at the lateral surface of a Taylor bubble is expected to be more efficient than that at the two ends because of higher relative velocity. Therefore, for the calculation of vapor generation, the interfacial area density due to the Taylor bubbles can be approximated as

$$a_{i,T} = \frac{4\,\alpha_T^{2/3}}{\alpha_{s\,max}^{1/6} D} \tag{24}$$

The advantage of the above expression is that it obviates the need for further adjustment of the parameter, λ_T.

The average void fraction of the bubbly-slug flow includes vapor volumes in the Taylor bubbles as well as the small bubbles. If the volume of a small bubble is denoted by V_b, then

$$\alpha = \frac{V_T + \Sigma V_b}{V_c} = \alpha_T + \alpha_b \tag{25}$$

where $\alpha_b = \Sigma V_b / V_c$ is the void fraction due to the small bubbles. At $\alpha = \alpha_{b\,max}$, $\alpha_b = \alpha_{b\,max}$ and $\alpha_T = 0$. At $\alpha = \alpha_{s\,max}$, $\alpha_b = 0$ and $\alpha_T = \alpha_{s\,max}$. Therefore, at $\alpha = \alpha_{s\,max}$, there will be a liquid film region of volume $(1 - \alpha_{s\,max})\,V_c$ with no bubbles. This leads to the idea of an "effective" volume of the bubbly mixture, which may be written as

$$V_{b,eff} = [\,V_c - f(1 - \alpha_{s\,max})\,V_c - V_T\,] \tag{26}$$

where $f = 0$ for $\alpha = \alpha_{b\,max}$,

and $f = 1$ for $\alpha = \alpha_{s\,max}$.

One possible expression for f is,

$$f = \frac{\alpha - \alpha_{b\,max}}{\alpha_{s\,max} - \alpha_{b\,max}} \tag{27}$$

Next, α_b' is defined as the void fraction due to the small bubbles on the basis of the "effective" volume of the bubbly mixture, i.e.,

$$\alpha_b' = \frac{\sum V_b}{V_{b,eff}} = \frac{\alpha_b}{1 - f\,(1 - \alpha_{s\,max}) - \alpha_T} \quad . \tag{28}$$

Consistent with the earlier assumption that bubble coalescence starts at $\alpha = \alpha_{b\,max}$, the local void fraction in the bubbly mixture of the bubbly-slug flow is assumed never to exceed $\alpha_{b\,max}$. Thus, as the average void fraction α increases beyond $\alpha_{b\,max}$, some small bubbles are removed from the bubbly region to form Taylor bubbles, and α_b' is bounded by $\alpha_{b\,max}$, i.e.,

$$\alpha_b' = \alpha_{b\,max} \quad . \tag{29}$$

Combining Equations (25) through (29), one obtains the following expression for α_T:

$$\alpha_T = \frac{(\alpha - \alpha_{b\,max})\;\alpha_{s\,max}}{(\alpha_{s\,max} - \alpha_{b\,max})} \tag{30}$$

Equation (30) together with Equation (24) provides the interfacial area density due to the Taylor bubbles alone. It was stated earlier that in the present study, $\alpha_{b\,max} = 0.3$ and $\alpha_{s\,max} = 0.8$.

Since most of the interface on the Taylor bubble is the lateral surface of the cylinder, this area is probably responsible for most of the heat transfer. The heat transfer coefficient to the cylindrical surfaces is approximated by that to liquid films. This approximation is the same as that used for the slug flow regime in TRAC-P1A code (24, 25). The following expression due to Linehan (26) is used in TRAC-P1A as well as in this study:

$$St_\ell = \frac{Nu_\ell}{Re_\ell\, Pr_\ell} = \text{constant} = 0.0073 \quad , \tag{31}$$

i.e., $h_T = 0.0073 \rho_\ell\, v_\ell\, c_{p\ell}$,

where $c_{p\ell}$ is the liquid specific heat.

The above correlation was obtained from condensation of steam over subcooled liquid film. Its direct application to the case of evaporation of liquid film may be questionable. In addition, the effect of vapor shear is not included. Therefore, the search for a better heat transfer correlation for Taylor bubbles should continue.

For the small bubbles in the bubbly-liquid mixture between two Taylor bubbles, the interfacial area density is given by:

$$a_{i,b} = \frac{3\,\alpha_b}{\omega_b} = \frac{3(\alpha - \alpha_T)}{\omega_b} \tag{32}$$

and the modified Aleksandrov equation, discussed earlier, continues to be used for the heat transfer coefficient.

The vapor drift velocity in the slug flow regime has been given by Zuber and Findlay (27), among others as

$$v_{gj,T} = 0.35\sqrt{\frac{g\,(\rho_\ell - \rho_g)\,D}{\rho_\ell}} \quad . \tag{33}$$

However, in the low void fraction range of the bubbly-slug regime, the flow field is still dominated by the small bubbles and not by the Taylor bubbles. Therefore, the relative velocity should still be influenced

mostly by the rise velocities of the small bubbles, with no discontinuous change in v_{gl}. Thus, the vapor drift velocity in bubbly-slug flow is assumed to be given by the following volume-averaged expressions:

$$v_{gj} = (\alpha_b v_{gj,b} + \alpha_T v_{gj,T}) / \alpha \quad (34)$$

and

$$v_{gl} = v_{gj} / (1 - \alpha) \quad (35)$$

where $v_{gj,b}$ is determined from Equation (8) and $v_{gj,T}$ from Equation (33). The relative velocity calculated from Equation (35) is then used in the calculation of the heat transfer coefficients h_b and h_T in the bubbly-slug regime.

Annular and Annular-Mist Flow

Annular and annular-mist flow take place in the transitional region between the bubbly-slug and the dispersed droplet regimes. As pointed out earlier, in the present model the flow pattern changes from the bubbly-slug regime to the pure annular flow regime at $\alpha = \alpha_{g\,max} = 0.8$. For pure annular flow, the interfacial area density and the heat transfer coefficient are given by:

$$a_i = \frac{4\alpha}{D} \quad (36)$$

and

$$h_l = 0.0073\, \alpha_l v_l \rho_{pl} \quad (37)$$

The situation becomes complicated as droplet entrainment begins. The onset of droplet entrainment may be determined from the correlations of Ishii and Grolmes (28). However, there are major uncertainties regarding the rate of entrainment and the sizes of droplets entrained in the vapor core. Further investigation is required in this area.

Dispersed Droplet Flow

When $\alpha > \alpha_d$, the liquid is assumed to be fully dispersed as droplets. The value of α_d is assumed to be 0.95. Alternatively, the exact value of α_d can be calculated from the model for the annular-mist flow as the liquid film at the wall dries out because of droplet entrainment and film evaporation. In the dispersed droplet regime, the droplet size may be expressed in terms of a critical droplet Weber number,

$$We_d = \frac{\rho_g v_{gl}^2 d}{\sigma} \quad (38)$$

Wallis (14) suggested the critical Weber number as 12 for droplets in a low viscosity carrier gas, whereas Gyarmathy (29) found the literature value of We_d in the range of 8 to 15. Wallis's value of 12 appears reasonable, therefore

$$d = \frac{12\sigma}{\rho_g v_{gl}^2} \quad (39)$$

Assuming spherical droplets, the interfacial area density can be given by:

$$a_{i,d} = \frac{6(1-\alpha)}{d} \quad (40)$$

Also, the relative velocity of the droplets can be given by:

$$v_{gl} = \frac{1.4}{\alpha}\left[\frac{g\sigma(\rho_l - \rho_g)}{\rho_g^2}\right]^{1/4} \quad (41)$$

The convective heat transfer to liquid droplets has been investigated by a number of researchers. Most of the data can be correlated by the expression

$$Nu_d = 2.0 + C_3 Re_d^{1/2} Pr_g^{1/3} \quad (42)$$

where the droplet Nusselt number is

$$Nu_d = h_d d / k_g \quad (43)$$

the droplet Reynolds number is

$$Re_d = \frac{\rho_g v_{gl} d}{\mu_g} \quad (44)$$

and the vapor Prandtl number is

$$Pr_g = \frac{c_{pg}\mu_g}{k_g} \quad (45)$$

In the above equations μ is the viscosity, k is the thermal conductivity, and subscript g refers to the vapor. Ranz and Marshall (30) found $C_3 = 0.6$ for various liquid or solid spheres in air or other fluids. Lee and Ryley (31) in experiments on evaporation of water droplets in superheated steam, found that $C_3 = 0.74$ for the Reynolds number range of 64 to 230. Since the two are close to each other and Lee and Ryley's correlation appears to be valid for droplet Reynolds numbers up to 40,000, Lee and Ryley's (31) correlation is used here for dispersed droplet flows.

COMPARISON WITH EXPERIMENTAL DATA

The present model has been applied to a steady-state flashing experiment conducted in a vertical converging-diverging Nozzle. The details of the experiment is given in Reference 11. The test section was made of stainless steel with a total length of 0.787m, including a symmetrical converging-diverging portion of 0.559m in length. The inside diameters at both ends were 0.051m and the throat inside diameter was 0.025m. Initially subcooled water at low pressures (2 to 8 bar) entered the test section at the bottom and flowed upwards. As the pressure decreased, flashing began near the throat and two-phase mixture flowed through the diverging part of the nozzle. Pressures and area-averaged void fractions were measured along the length of the test section. The accuracy of the pressure measurement was within 1% of the reading and that for the void fraction was within 0.05. The accuracy for the fluid temperature measurement was within 0.1°C.

A computer program was written for the present model described earlier. Steady-state balance equations for mass and energy were employed. No momentum equation was used; instead, the experimental pressure distribution was imposed. Since the maximum void

fraction in the experiments simulated was less than 0.8, only the models developed for the bubbly and the bubbly-slug regimes were programmed. The following mixture mass and mixture energy equations were used for both of these regimes:

$$GA = \text{constant} \tag{46}$$

and

$$h_m + \frac{1}{2}\left(\frac{G}{\rho_m}\right)^2 = \text{constant} \tag{47}$$

Assuming the vapor phase to be at saturation, the specific enthalpy for the liquid phase was calculated by

$$h_\ell = \frac{h_m - c h_g}{(1-c)} \tag{48}$$

where c is the vapor mass concentration and is defined by $c = \alpha\rho_g/\rho_m$. The liquid superheat was then calculated from

$$T_\ell - T_{sat} = \frac{h_\ell - h_f}{c_{p\ell}} \ . \tag{49}$$

For void fraction calculation, Equations (15) through (17) were used for the bubbly flow regime where bubbles were tracked as they grew. However, in the bubbly-slug regime, a more general form of the vapor mass equation was used. The equation employed was:

$$G\frac{dX}{dZ} = \Gamma_v = \frac{(h_T a_{i,T} + h_b a_{i,b})(T_\ell - T_{sat})}{L} \tag{50}$$

The void fraction was then calculated from

$$\alpha = \frac{X}{\left[X + (1-X)\rho_g/\rho_\ell\right] + \rho_g v_{gj}/G} \tag{51}$$

For a given simulation, the input consisted of:

1. The effective geometry of the converging-diverging nozzle (11).
2. The nozzle inlet conditions, i.e., pressure temperature, and velocity or flow rate.
3. The experimental pressure distribution along the length of the nozzle (11).

For all the runs considered here, the flashing inception point was taken to be at the nozzle throat. This is based on the experimental void fraction data as well as the study of Abuaf, et al. (11, 32) which showed that the flashing inception point according to the Alamgir-Lienhard correlation (9) was indeed very close to or at the nozzle throat. The critical bubble radius at the throat pressure was calculated by using Equation (3), and a bubble number density at the inception point, $N_{b,o}$, was assumed to start the calculation. A marching technique was used to calculate all the variables (except pressure) along the length of the nozzle. Axial steps or mesh sizes were small enough to assure a converged result. The axial void fraction profile calculated by the computer program was then compared with the area-averaged void fraction data. In case of unsatisfactory agreement, the free parameter, $N_{b,o}$, was varied until a "best-fit" between the calculated and the measured void fractions was obtained.

A total of 15 runs were simulated with the present model. They can be grouped under the following four sets:

1. Runs 353,358, and 362, all with approximately the same inlet water temperature of 100°C, but with increasing mass flow rates.
2. Runs 145, 133, 137, and 344, all with approximately the same inlet water temperature of 121°C, but with increasing mass flow rates.
3. Runs 291, 284, 273, 278, and 296, all with approximately the same inlet temperature of 149°C, but with increasing mass flow rates.
4. Runs 268, 304, and 309, with approximately the same inlet water temperature of 149°C and the same mass flow rate, but with decreasing exit pressure.

Some results of the calculation with the "optimum" values of bubble number density at the inception point are shown in Figures 3 through 5. It can be noticed that the agreement in the bubbly flow regime, i.e., $\alpha < 0.3$, is quite reasonable. However, there is still room for improvement in the bubbly-slug regime, i.e., $0.3 < \alpha < 0.8$. Further examination of the interfacial area and heat transfer models used in this regime is required. This includes extending the bubbly flow regime up to a void fraction of 0.4 or 0.5, as suggested by the comparisons.

Table 1 provides a summary of the test conditions and the optimum values of the bubble number density at the flashing inception point. No clear cut relationship between the mass flow rate and the liquid superheat at the flashing inception point can be found. However, when the optimum values for the bubble number density at the inception point, $N_{b,o}$, are plotted against the liquid superheat at the inception point, $\Delta T_{\ell,o}$, a clear trend can be found as shown in Figure 6. The optimum number of bubbles at the inception point seems to increase until a liquid superheating of 3°C is reached. Thereafter, the heat transfer rate to the interface is so large that fewer number of bubbles are needed to be nucleated as the liquid superheating at the inception point increases. The phenomenon can be better understood when the interfacial area density at the inception point, i.e., $a_{i,o}$, which is equal to $4\pi R_{cr}^2 N_{b,o}$, is plotted against the liquid superheating at the inception point. This is shown in Figure 7. It is interesting to note that although the bubble number density decreased as the liquid superheating dropped below 3°C, the interfacial area density continued to increase monotonically as the liquid superheating decreased even below 3°C. This is consistent with the requirement that as the flow approaches a thermal equilibrium flow, i.e., $\Delta T_\ell \to 0$, the interfacial area for heat and mass transfer must approach infinity. It should also be noted that as $\Delta T_\ell \to 0$, the critical bubble radius $R_{cr} \to \infty$. Therefore, the bubble number density, $N_{b,o}$, does not have to approach infinity as $\Delta T_{\ell,o} \to 0$. This explains the apparent contradiction between Figures 6 and 7.

Although Figure 6 may serve as a guidance for the selection of the optimum bubble number density at the inception point once that point is determined, it must be realized that the data base for Figure 6 is quite limited. Only one nozzle size was used, and the

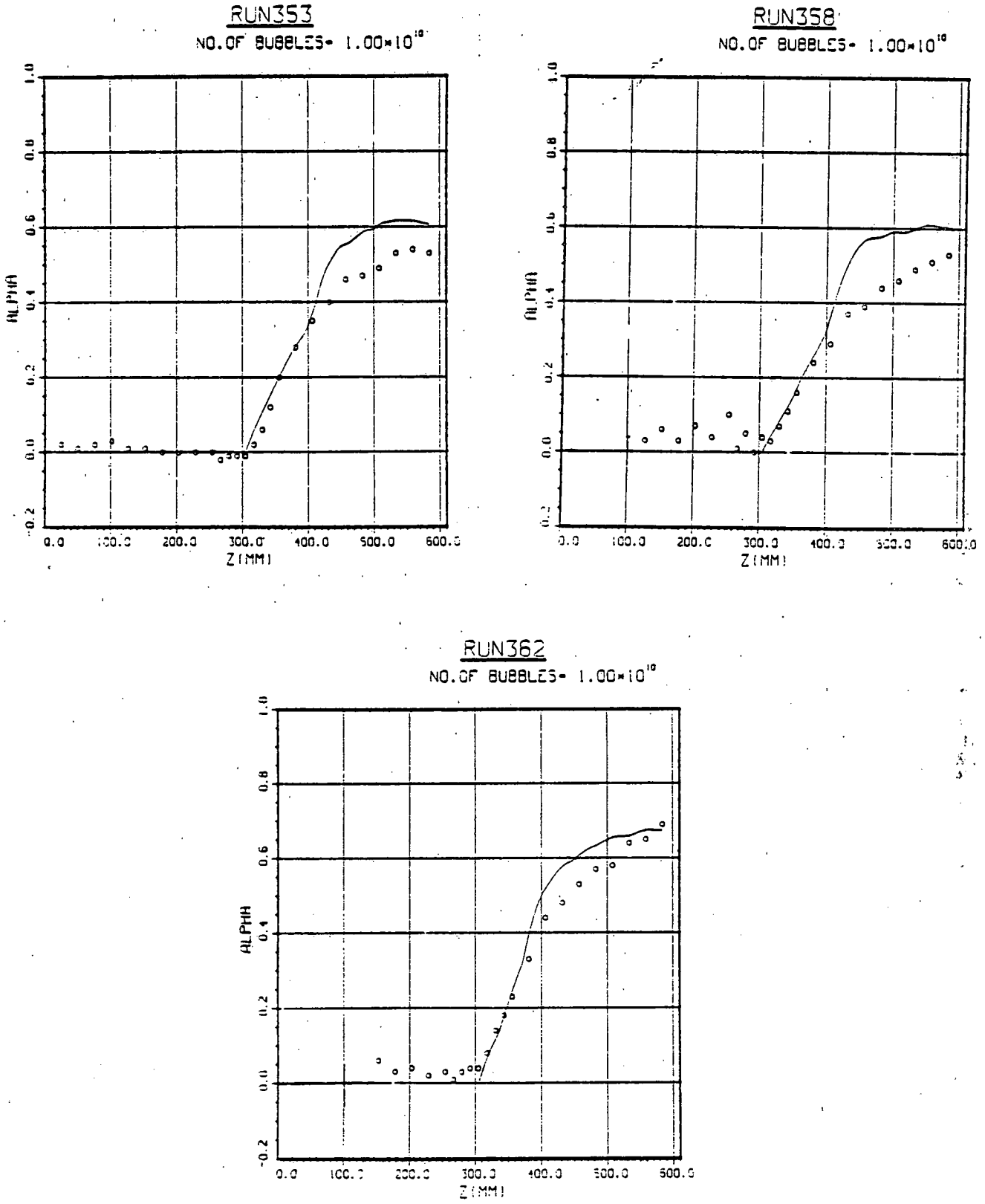

Figure 3. Comparison Between the Void Fraction Data for Runs 353, 358, and 362 and the "Best-Fit" Calculations Using the Present Model.

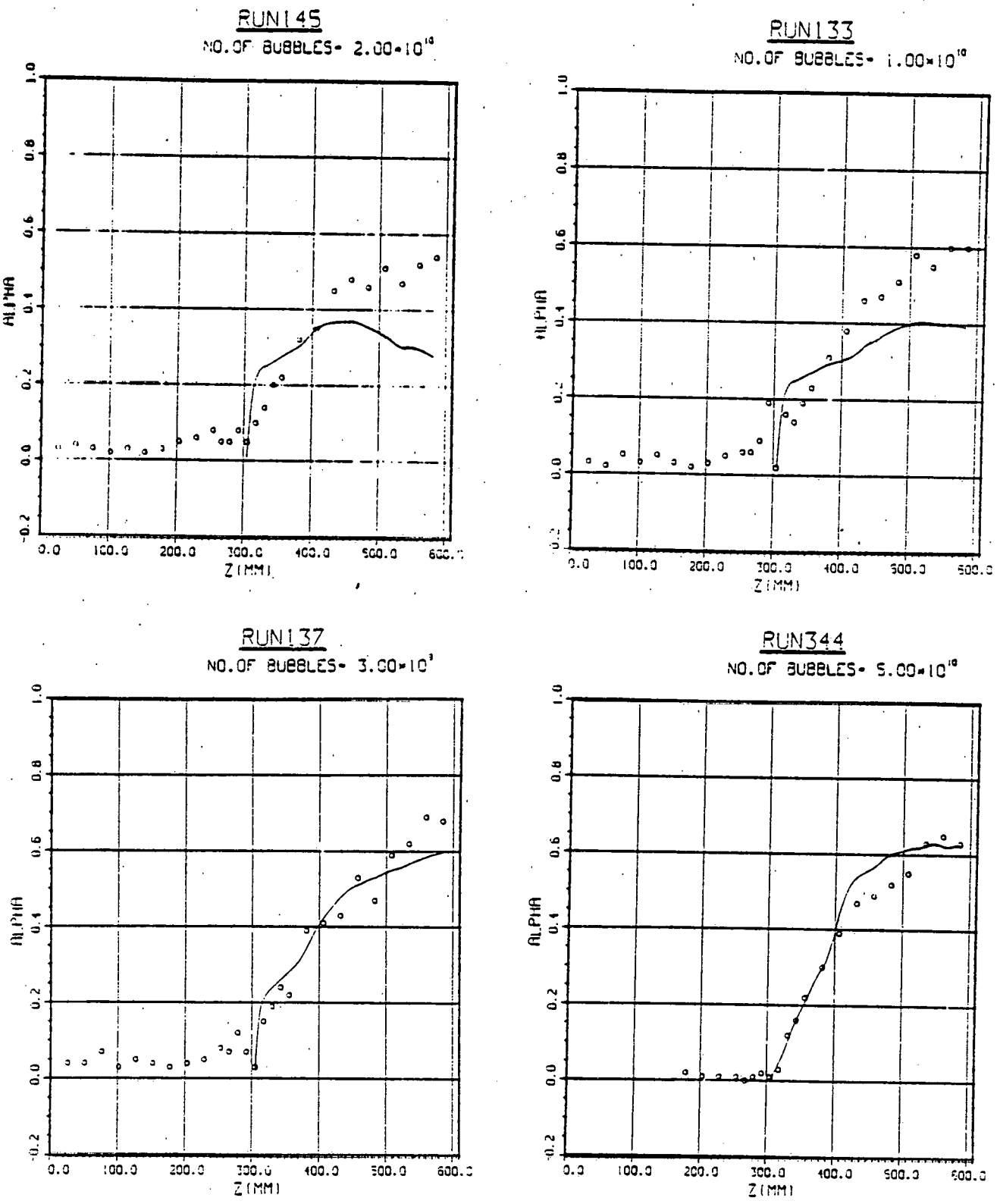

Figure 4. Comparison Between the Void Fraction Data for Runs 145, 133, 137, and 344 and the "Best-Fit" Calculations Using the Present Model.

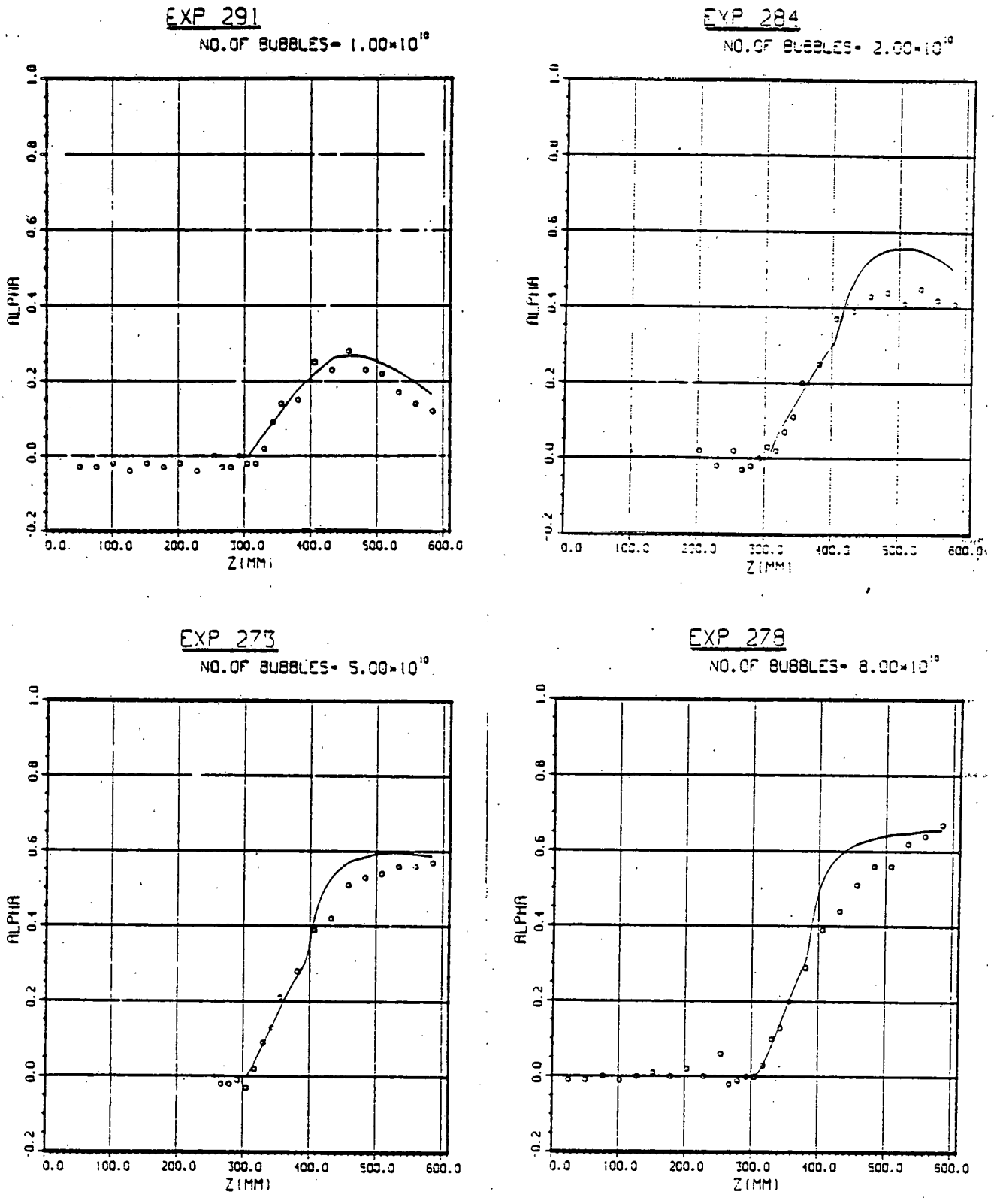

Figure 5. Comparison Between the Void Fraction Data for Runs 291, 284, 273, and 278 and the "Best-Fit" Calculations Using the Present Model.

Table 1. Summary of Test Conditions and Present Model Calculations*

Run No.	T_{in} (°C)	G_o (kg/m^{2}s)	P_o (bar)	$\Delta T_{l,o}$ (°C)	$N_{b,o}$ (No/m^3)	R_{cr} (um)	$a_{i,o}$ (m^2/m^3)
353	100.0	18974	0.955	1.65	1×10^{10}	20.3	25.5
358	100.0	25116	0.950	1.80	1×10^{10}	18.7	23.5
362	99.7	28314	0.929	2.13	1×10^{10}	16.3	20.27
145	121.2	13566	1.742	5.31	2×10^{10}	3.48	3.043
133	121.2	18658	1.634	7.28	1×10^{10}	2.63	0.865
137	121.2	24801	1.482	11.32	0.3×10^{10}	1.71	0.11
344	121.3	27935	1.922	2.23	5×10^{10}	7.88	39.0
291	148.9	13336	4.03	5.0	1×10^{10}	1.71	0.367
284	149.2	13061	4.047	5.2	2×10^{10}	1.63	0.557
273	148.7	18048	4.192	3.4	5×10^{10}	2.46	3.79
278	148.7	24119	4.257	2.34	8×10^{10}	2.82	8.04
296	148.8	27148	4.17	3.7	8×10^{10}	2.27	4.52
268	148.9	18091	4.057	4.91	3×10^{10}	1.73	1.13
304	148.9	18133	3.997	5.25	4×10^{10}	1.64	1.35
309	149.1	18217	3.935	6.12	0.5×10^{10}	1.41	0.125

* The subscript "o" refers to the flashing inception point.

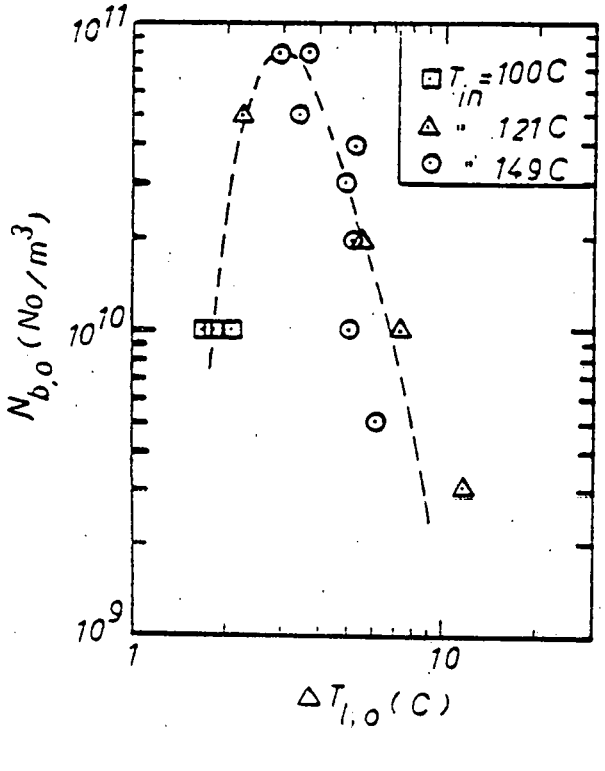

Figure 6. The Optimum Bubble Number Density at the Inception Point vs. the Liquid Superheat at the Inception Point.

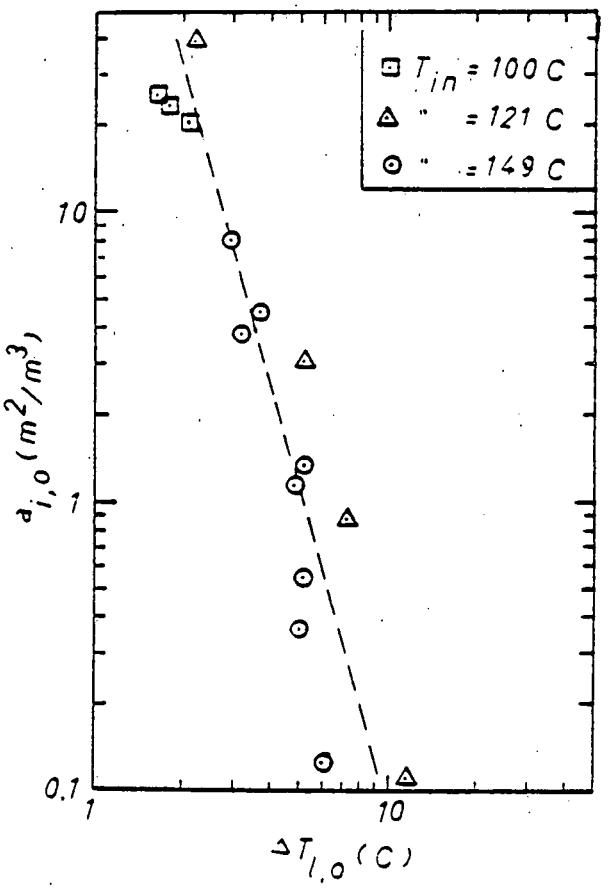

Figure 7. The Interfacial Area Density at the Inception Point vs. the Liquid Superheat at the Inception Point.

experiments were conducted only at low pressures and temperatures. Therefore, the data base must be expanded first to develop a general correlation for the bubble number density or the interfacial area density at the inception point. Furthermore, the model for the bubbly-slug flow regime should be improved, and the same for the annular-mist flow has to be developed.

SUMMARY AND CONCLUSION

1. A model of vapor generation following flashing inception has been proposed including the interfacial area density, heat transfer coefficients for vaporization and the relative velocity in all flow regimes covering the void fraction range $0 < \alpha < 1.0$. The model for annular-mist flow has not yet been completed although a general direction has been specified.

2. Since most of the nozzle data with which the model was compared are within $0 < \alpha < 0.3$, this lack of a definite model for the annular-mist flow did not pose any problem.

3. Comparison of the model predictions with the experimental area-averaged void fraction distributions obtained in a vertical converging-diverging nozzle showed a reasonable agreement in the bubbly flow regime. However, there is still room for improvement in the bubbly-slug regime.

4. The optimum bubble number density at inception, $N_{b,o}$, determined from "best-fit" considerations, increased with the liquid superheat at inception, $\Delta T_{\ell,o}$, until a liquid superheat of 3°C was reached. The bubble number density decreased as the liquid superheat increased beyond 3°C.

5. The interfacial area density calculated from the critical bubble radius and the optimum bubble number density at inception increased monotonically with a decreasing liquid superheat. This trend is consistent with the interfacial area requirement for a thermal equilibrium flow.

ACKNOWLEDGEMENTS

The authors would like to thank Mrs. Y. Sanborn for her help in developing and running the computer program used for this study. Typing of Mrs. J. V. Muller and Ann C. Fort is also appreciated.

REFERENCES

1 Jones, O.C.,Jr., and Saha, P., "Nonequilibrium Aspects of Water Reactor Safety," in Symposium on the Thermal and Hydraulic Aspects of Nuclear Reactor Safety Vol. 1: Light Water Reactors, O.C. Jones, Jr. and S.G. Bankoff editors, ASME, 1977, pp. 249-288.

2 Wegener, P.P., and Wu, B.J.C., "Gasdynamics and Homogeneous Nucleation," in Nucleation Phenomena, A.C. Zettlemoyer editor, Elsevier, New York,1977,p.325.

3 Oswatitsch, J., "Kondensationserscheinungen in Ubverschalldusen," Z. angew. Math. Mech. Vol. 22, 1942, p. 1.

4 Zuber, N., Staub, F.W., and Bijwaard, G., "Vapor Void Fraction in Subcooled Boiling and in Saturated Boiling Systems," Proc. 3rd Int. Heat Trans. Conf., Vol. 5, 1966, p. 24.

5 Rohatgi, U.S., and Reshotko, E., "Nonequilibrium One-Dimensional Flow in Variable Area Channels," Nonequilibrium Two Phase Flow, R.T. Lahey, Jr., and G.B. Wallis editors, ASME, 1975, pp. 47-54.

6 Simoneau, R.J., "Pressure Distribution in a Converging-Diverging Nozzle During Two-Phase Choked Flow of Subcooled Nitrogen," NASA TMX-71762, 1975.

7 Wu, B.J.C., Saha, P., Abuaf, N., and Jones, O.C., Jr., "A One-Dimensional Model of Vapor Generation in Steady Flashing Flow," BNL-NUREG-25709, 1979. Also, ANS Transactions, Vol. 32, 1979, pp. 490-491.

8 Reocruex, M., "Contribution a l'etude des Debits Critiques en Ecoulement Diphasique Eau-Vapeur," PhD Thesis, Universite Scientifique et Medicale de Grenoble, France, 1974.

9 Alamgir, Md., and Lienhard, J.H., "Correlation of Pressure Undershoot During Hot-Water Depressurization," Journal of Heat Transfer, Vol. 103, February 1981, pp. 52-55.

10 Lackme, C., "Autovaporisation Dans une Conduite d'un Liquide Satre ou Sous-Refroidi a l'Entree, CEA-R-4957, 1979.

11 Abuaf, N., Zimmer, G.A., Wu, B.J.C., and Saha, P., "A Study of Nonequilibrium Flashing of Water in a Converging-Diverging Nozzle," BNL-NUREG-51317, NUREG/CR 1864, 1981.

12 Jones, O.C.,Jr., and Zuber, N., "Evaporation in Variable Pressure Fields," Journal of Heat Transfer, Vol. 100, 1978, pp. 453-459.

13 Edwards, A.R., "Conduction Controlled Flashing of a Fluid, and the Prediction of Critical Flow Rates in One-Dimensional System," U.K. Atomic Energy Authority Report, AHSB (S) R 147, 1968.

14 Wallis, G.B., One-Dimensional Two-Phase Flow, McGraw-Hill, N.Y., 1969, Chapters 9 and 12.

15 Saha, P., "Analytical Modeling: Effect of Pressure Change," in Reactor Safety Research Program, Quarterly Progress Report for the Period April - June 1977, BNL-NUREG-50683, 1977, pp. 145-155.

16 Plesset, M.S., and Zwick, S.A., "The Growth of Vapor Bubbles in Superheated Liquids," Journal of Applied Physics, Vol. 25, No. 4, 1954, pp. 493-500.

17 Forster, H.K., and Zuber, N., "Growth of a Vapor Bubble in a Superheated Liquid," Journal of Applied Physics, Vol. 25, No. 4, 1954, pp. 474-478.

18 Wolfert, K., "The Simulation of Blowdown Processes with Consideration of Thermodynamic Nonequilibrium Phenomena," Paper presented at OECD Specialist's Meeting on Transient Two-Phase Flow, Toronto, 1976.

19 Chao, B.T., "Transient Heat and Mass Transfer to a Translating Droplet," Journal of Heat Transfer, Vol. 91, 1969, p. 273.

20 Davenport, W.G., Richardson, F.D., and Bradshaw, A.V., "Spherical Cap Bubbles in Low Density Liquids," Chemical Engineering Science, Vol. 22, 1967, p. 1221.

21 Calderbank, P.H., and Lochiel, A.C., "Mass Transfer Coefficients, Velocities and Shapes of Carbon Dioxide Bubbles in Free Rise Through Distilled Water," Chemical Engineering and Science, Vol. 19, 1964, p. 485.

22 Aleksandrov, Y.A., Voronov, G.S., Gorbunkov, V.M., Delone, N.B., and Nechayev, Yu,I., Bubble Chambers, Indiana University Press, Bloomington, Ind. 1967, pp. 72-76.

23 Dukler, A.E., and Taitel, Y., "Flow Regime Transitions for Vertical Upward Gas-Liquid Flow: A Preliminary Approach Through Physical Modeling," NUREG-0162, 1977.

24 TRAC-PlA, An Advanced Best-Estimate Computer Program for PWR LOCA Analysis, Los Alamos Scientific Laboratory Report LA-7777-MS, NUREG/CR-0665, May 1979.

25 Rohatgi, U.S., and Saha, P., "Constitutive Relations in TRAC-PlA," NUREG/CR-1651, BNL-NUREG-51258, 1980, pp. 6-8.

26 Linehan, J.H., "The Interaction of Two-Dimensional, Stratified, Turbulent Air-Water and Steam Water Flows," ANL-7444, 1968.

27 Zuber, N., and Findlay, J., "Average Volumetric Concentration in Two-Phase Flow Systems," Journal of Heat Transfer, Vol. 87, 1965, p. 453.

28 Ishii, M., and Grolmes, M.A., "Inception Criteria for Droplet Entrainment in Two-Phase Concurrent Film Flow," AIChE Journal, Vol. 21, 1975, pp. 308-318.

29 Gyarmathy, G., Two Phase Steam Flow in Turbines and Separators, Edited by M.J. Moore and C.H. Sieverding, McGraw-Hill, N.Y., 1979, pp. 49-50.

30 Ranz, W.E., and Marshall, W.R., "Evaporation from Drops," Chemical Engineering Progress, Vol. 48, 1952, pp. 144-146 and 173-180.

31 Lee, J., and Ryley, D.J., "The Evaporation of Water Droplets in Superheated Steam," Journal of Heat Transfer, Vol. 90, 1968, p. 445.

32 Abuaf, N., Jones, O.C.,Jr., and Wu, B.J.C., "Critical Flashing Flows in Nozzles with Subcooled Inlet Conditions," BNL-NUREG-27512, 1980.